

Structural variation in a synchrotron-induced contamination layer (a-C:H) deposited on a toroidal Au mirror surface

P. K. Yadav,^{a,b*} R. K. Gupta,^a M. K. Swami^c and M. H. Modi^a

^aSoft X-ray Applications Laboratory, Raja Ramanna Centre for Advanced Technology, Indore 452013, India,

^bHomi Bhabha National Institute, Bhabha Atomic Research Centre, Anushakti Nagar, Mumbai 400094, India, and

^cLaser Biomedical Applications Section, Raja Ramanna Centre for Advanced Technology, Indore 452013, India.

*Correspondence e-mail: praveenyadav@rrcat.gov.in

Received 10 March 2017

Accepted 15 May 2017

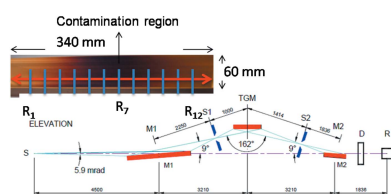
Edited by A. Momose, Tohoku University, Japan

Keywords: reflectivity; Raman spectroscopy; X-ray diffraction; hydrogenated carbon.

A carbon layer deposited on an optical component is the result of complex interactions between the optical surface, adsorbed hydrocarbons, photons and secondary electrons (photoelectrons generated on the surface of optical elements). In the present study a synchrotron-induced contamination layer on a 340 mm × 60 mm Au-coated toroidal mirror has been characterized. The contamination layer showed a strong variation in structural properties from the centre of the mirror to the edge region (along the long dimension of the mirror) due to the Gaussian distribution of the incident photon beam intensity/power on the mirror surface. Raman scattering measurements were carried out at 12 equidistant (25 mm) locations along the length of the mirror. The surface contamination layer that formed on the Au surface was observed to be hydrogenated amorphous carbon film in nature. The effects of the synchrotron beam intensity/power distribution on the structural properties of the contamination layer are discussed. The $I(D)/I(G)$ ratio, cluster size and disordering were found to increase whereas the $sp^2:sp^3$ ratio, G peak position and H content decreased with photon dose. The structural parameters of the contamination layer in the central region were estimated (thickness $\simeq 400$ Å, roughness $\simeq 60$ Å, density $\simeq 72\%$ of bulk graphitic carbon density) by soft X-ray reflectivity measurements. The amorphous nature of the layer in the central region was observed by grazing-incidence X-ray diffraction.

1. Introduction

Long-term operation of synchrotron beamlines results in optics contamination by hydrocarbon molecules present in beamline vacuum chambers. Even in ultra-high-vacuum environments of beamlines the hydrocarbon gases (CO, CO₂, CH₄ etc.) with a partial pressure of 10⁻¹⁰ torr form a monolayer on the surface of the mirror in approximately 2–3 h. A typical residual gas analyzer spectrum of the soft X-ray reflectivity beamline of Indus-1 in the 1 to 50 a.m.u. range is shown in Fig. 1. The presence of hydrocarbon molecules at 10⁻¹¹ to 10⁻⁹ torr is clearly indicated. When synchrotron radiation falls on adsorbed hydrocarbon molecules on a mirror surface, dissociation of the adsorbed molecules takes place at the mirror surface by synchrotron radiation as well as by secondary electrons generated at the mirror surface. Boller *et al.* reported that the deposition can be explained as a cracking of hydrocarbon molecules by secondary electrons (*i.e.* photoelectrons) from the surface upon irradiation (Boller *et al.*, 1983; Leontowich & Hitchcock, 2012), while Hollenshead & Klebanoff claimed that bond breaking of hydrocarbons is dominated by direct photon absorption rather than



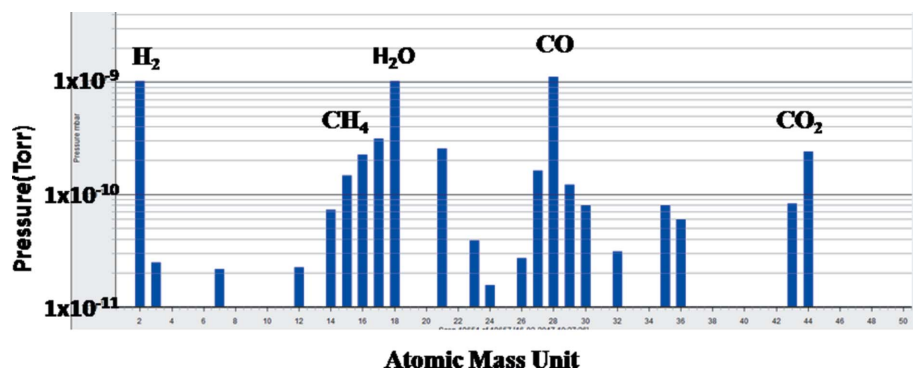


Figure 1
Typical residual gas analyzer spectrum from the reflectivity beamline at Indus-1 in the presence of a zero-order photon beam at 80 mA electron beam current.

exposure to secondary electrons. The dissociated hydrocarbon atoms or molecules cross-link and accumulate at the surface of the mirror (Hollenshead & Klebanoff, 2006). Continuous cross-linking and accumulation forms a continuous thick and rough layer of carbon, which is undesirable for the reflective optics. Surface diffusion of hydrocarbon molecules towards the irradiated area also contributes to the layer thickness (Ellis, 1951; Hart *et al.*, 1970). The precise mechanism of the deposition process is still being debated.

The actual form of carbon deposited on optical elements after dissociation of hydrocarbon molecules by synchrotron radiation is also not well known because the properties of the contamination layer vary with the amount of hydrogen present and hybridization states (sp^3 , sp^2 and sp^1) ratios in the layer structures. Ferrari & Robertson explained the form of carbon by the presence of H, sp^2 and sp^3 content using ternary phase diagrams (Ferrari & Robertson, 2004). The sp^2 hybridized (graphitic-like) carbon (GLC) itself has many forms ranging from micro-crystalline graphite to glassy carbon. Diamond-like carbon (DLC) is an amorphous carbon (a-C)/(a-C:H) with a significant fraction of sp^3 bonds. Film with the same sp^3 and H content but different sp^2 clustering and orientation can have different optical, electronic and mechanical properties (Robertson, 2002). The clustering and orientation of sp^2 or sp^3 and content of H may vary by annealing and continuous exposure by photons and electrons/ions. Faradzhev *et al.* analyzed the photo-induced (extreme-ultraviolet radiation) carbonaceous layer grown on a TiO_2 thin film using X-ray-excited valence-band spectra and gas chromatography/mass spectroscopy (GC/MS). They observed that, under continuing irradiation, EUV-induced dehydrogenation and cross-linking of polycyclic aromatic hydrocarbon (PAH) and precursor alkane fragments form a complex network of carbon bonds with the inferred structure of an sp^2 carbon-rich film (Faradzhev *et al.*, 2013). Conway *et al.* observed dispersion in the G-peak in an annealing cycle up to 1000°C for hydrogenated tetrahedral amorphous carbon (ta-C:H) film. The G-peak is a representation of carbon in the sp^2 hybridization state; it is not a matter that it is arranged in chains or rings (Conway *et al.*, 2000). Dispersion in the G-peak occurs due to amorphization or crystallization of carbon atoms in film and H

content (Ferrari & Robertson, 2004). Choi & Hattta (2015) observed structural change in hydrogenated amorphous carbon films (a-C:H) due to hydrogen evolution and thermal relaxation in the films by electrons/ion intensity variation. We also studied a contamination layer on a LiF window deposited by vacuum ultraviolet radiation, and observed that the layer has graphitic carbon-like and polymer-like characteristics (Yadav *et al.*, 2016).

The present sample (contamination layer/Au mirror) is a result of continuous exposure of the Au mirror by photons in the energy range from the infrared to the soft X-ray. At the critical wavelength (61 Å) the photon flux is about 10^{10} photons s^{-1} $mrad^{-1}$ (0.1% bandwidth) $^{-1}$. A typical beam profile at the critical wavelength (61 Å) on the mirror surface is simulated by ray-tracing program and shown in Fig. 2. The beam profile indicates that the photon intensity is maximum at the centre and it decreases gradually along the length of the mirror. It is expected that, due to the photon intensity distribution on the mirror surface, the properties of the contamination layer should vary along the length direction. In order to characterize the deposited layer, the mirror surface is sampled at 12 equidistant (25 mm) locations along its length by Raman scattering measurement. In the central region structural parameters are measured by soft X-ray reflectivity measurement. The amorphous/crystalline nature of the layer is confirmed by grazing-incidence X-ray diffraction.

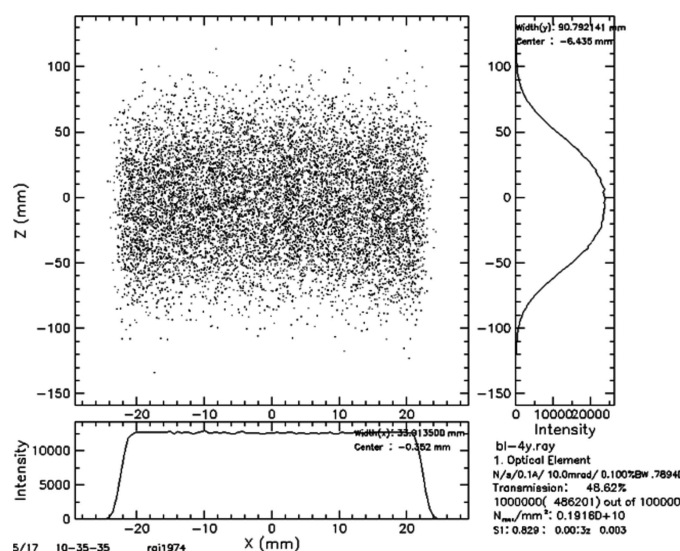


Figure 2
Synchrotron radiation beam profile on the mirror surface simulated by ray-tracing program. Input parameters are: wavelength, 61 Å; horizontal and vertical beam acceptance, 10 mrad and 5.9 mrad, respectively; source-to-mirror distance, 4500 mm.

This carbon contamination layer on mirrors reduces the photon flux near the carbon K -absorption edge (284 eV). In the case of multi-element optical systems, even a very thin layer of carbon on the top of each optical element reduces the reflected photon flux significantly. The deposited layer is not uniform because the photon beam profile is Gaussian in nature; as a result, the layer thickness is high in the central region of the beam exposure area. This additional carbon layer produces a phase difference $\Delta\Phi = (2\pi\delta/\lambda)d_c$, where δ is the dispersive optical constant at wavelength λ and d_c is the carbon layer thickness. This phase difference can lead to destructive interference at certain wavelengths. The increase in roughness also exponentially decreases the reflected photon flux [$R = R_0 \exp(-q^2\sigma^2)$, where R is the reflected intensity, q and σ are the momentum transfer and surface roughness, respectively]. The magnitudes of s and p polarization are also affected by the carbon layer.

Before refurbishing the optics (online or offline) it is better to determine the phase of carbon and its distribution on the surface of the optics. The denser structure of DLC film is likely to be more difficult to clean by the UV/O₃ cleaning method and any other conventional method because the carbon in DLC form is more tightly bound. Several beamline users face the carbon-contamination problem and various online and offline cleaning mechanisms are investigated for refurbishing contaminated optics.

2. Experimental details

2.1. Sample for study

For the present study, a synchrotron-radiation-induced contaminated gold-coated toroidal mirror (M1; contamination layer Au/Cr/SiO₂) of the soft X-ray reflectivity beamline of Indus-1 is used. The dimensions of the mirror are 340 mm × 60 mm (shown in Fig. 3). This mirror is the first optical element

towards the source side; as a result, the full mirror is exposed to photons of all energies generated by the source. The distance of M1 from the source is 4500 mm. Photons from the source fall directly onto the mirror at a 4.5° incidence angle. The acceptance angles of the mirror are 10 mrad in the horizontal and 5.9 mrad in the vertical direction. A typical optical layout of the beamline is shown in Fig. 3. The contamination layer formed on the mirror surface used for the present study is a result of the exposure of 577 mW power for an average of 4 h per day for a ten year duration (this includes photons of all energies ranging from infrared to soft X-ray) at 10⁻⁹ torr pressure. Due to the Gaussian beam profile the photon intensity is maximum at the centre and gradually decreases moving outwards.

2.2. Characterization

Raman spectra from the sample surface were recorded at room temperature by Alpha 300SR Witec Instruments (GmbH Germany) using 441.6 nm lines of a He–Cd laser as excitation source. The laser light is coupled to a single mode fiber for delivering light to the microscope. The Raman signal was collected using a 50× [0.55 numerical aperture (NA)] microscope objective and coupled to a 100 μm (0.11 NA) multimode optical fiber. The multimode optical fiber is coupled to an Acton 2500i spectrometer (Princeton Instruments, USA). Twelve Raman spectra (R-1 to R-12) with 25 mm intervals along the mirror length were acquired using a TE-cooled (−72°C) CCD (ANDOR 420BR DD) in the spectral region 175–3600 cm⁻¹ at 4 cm⁻¹ resolution. The spot size of the laser beam on the sample surface was about 2 μm. A low input power (≤5 mW) was used in order to avoid any heating damage on the sample surface.

Reflectivity (θ – 2θ) data sets at three different wavelengths (80, 90 and 100 Å) were acquired at the Indus-1 soft X-ray reflectivity beamline (Nandedkar *et al.*, 2002) in a high vacuum

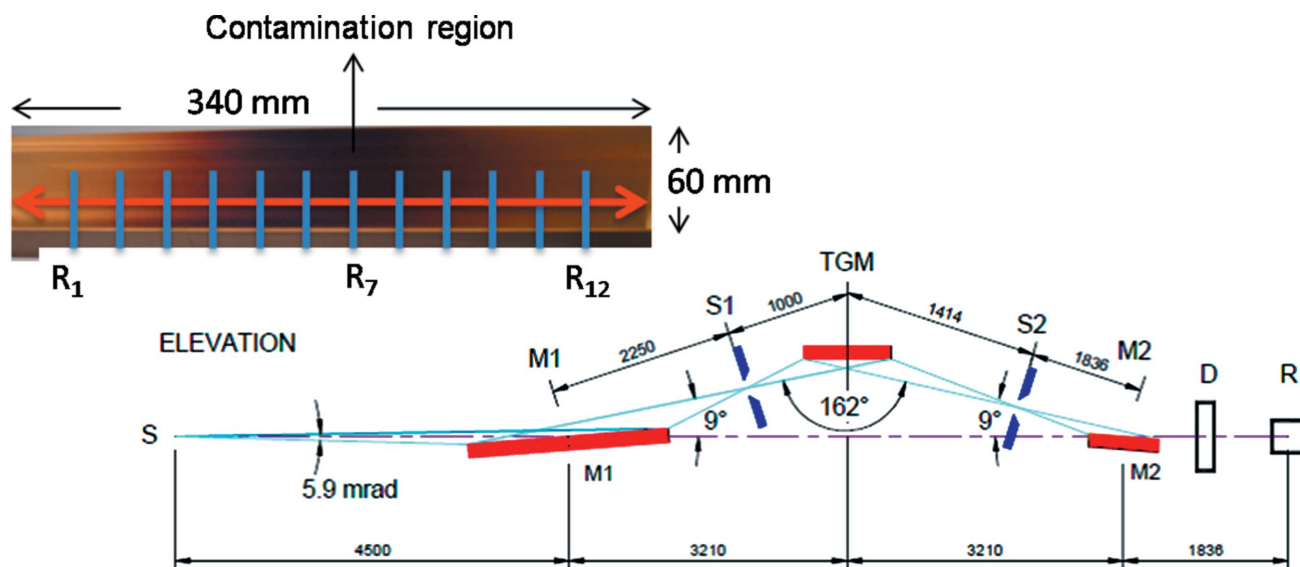


Figure 3

Optical layout of the reflectivity beamline at the Indus-1 source with a zoomed image of the carbon-contaminated Au-coated mirror. The vertical lines on the mirror indicate measurement positions labeled R₁ through R₁₂.

of 10^{-7} torr. The photon energy was calibrated by measuring the absorption spectrum of Si near the *L*-absorption edge. The reflectivity experiments were carried out at the centre position of the contaminated Au mirror, marked as R₇ on mirror surface (see Fig. 3). The $(\theta-2\theta)$ scan was taken from 0 to 50° with a step size of 0.08° in θ . The measured reflectivity was fitted by the Parratt recursive formalism that is based on Fresnel reflection equations (Parratt, 1954). Fitted and measured reflectivity *versus* momentum transfer ($q = 4\pi \sin \theta/\lambda$) and the corresponding optical density profiles are shown in Figs. 4(a) and 4(b), respectively. From the reflectivity data fitting, the structural parameters of the carbon layer (thickness ~ 400 Å, roughness 60 Å and density $\sim 72\%$ of graphitic carbon density) from the dispersive part of the optical constant (δ) in the central region (R₇) were obtained {the dispersive part δ is directly related to the density of material [$\delta = (n_a r_e \lambda^2 f_1)/2\pi$], where n_a is the atomic density, r_e is the classical electron radius, λ is the incident wavelength and f_1 is real part of the atomic structure factor} (Attwood, 1999).

In order to determine the crystalline or amorphous nature, grazing-incidence X-ray diffraction (GIXRD) was carried out at the angle-dispersive X-ray diffraction (ADXRD) beamline (Sinha *et al.*, 2013). An energy of 11.39 keV was chosen using the double-crystal monochromator at the Indus-2 synchrotron radiation source. The angle of incidence was kept at 1° with respect to the sample surface and the detector was moved from 10° to 45° in steps of 0.04°. Two diffraction peaks of Au, (111) and (200), and the broad hump of amorphous carbon (a-c) were observed at 26.7°, 30.95° and 14.8°, respectively. The diffracted pattern is shown in Fig. 5. In order to find out the cluster/grain size of amorphous carbon, Gaussian peak fitting was performed (inset in Fig. 5). The out-of-plane grain size of carbon, ~ 11.7 Å, was calculated using the well known Scherrer equation.

3. Results and discussion

A contamination layer deposited on a Au surface by complex interaction among hydrocarbon gas molecules with photons

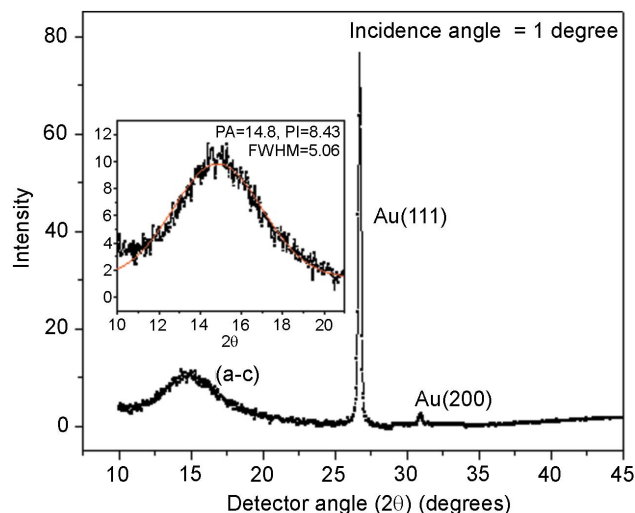


Figure 5 Grazing-incidence X-ray diffraction of the contaminated Au-coated toroidal mirror. The inset shows the Gaussian fitting of the a-c peak.

and secondary electrons has been analyzed by Raman spectroscopy, soft X-ray reflectivity and GIXRD measurements. As we discussed earlier, the exact process of deposition and the phase of the carbon layer are not well known and are still debatable. Raman spectroscopy is a comparatively simple and non-destructive technique and is very sensitive for carbon-based materials that involve no special specimen preparation. Fig. 6(a) shows 12 (R-1 to R-12) Raman spectra of the deposited contamination layer. The spectra were recorded at equal distances (25 mm) from one end to the other as shown by vertical lines in Fig. 3. Spectrum R-7 is from the central region (dense contamination region) whereas R-1 and R-12 are from near the edges of the mirror. The spectra cover 175 cm^{-1} to 3700 cm^{-1} with a resolution of 4 cm^{-1} . In order to analyze the spectra quantitatively, the raw data are normalized by subtracting a linear background. Raman spectra are deconvoluted to two Lorentzian functions in the 900 cm^{-1} to 2000 cm^{-1} region. The spectra clearly show the G

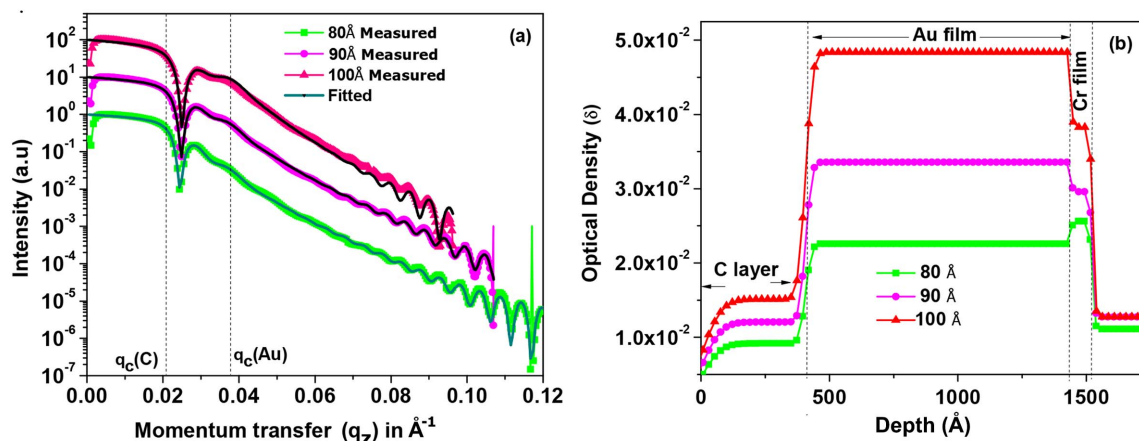
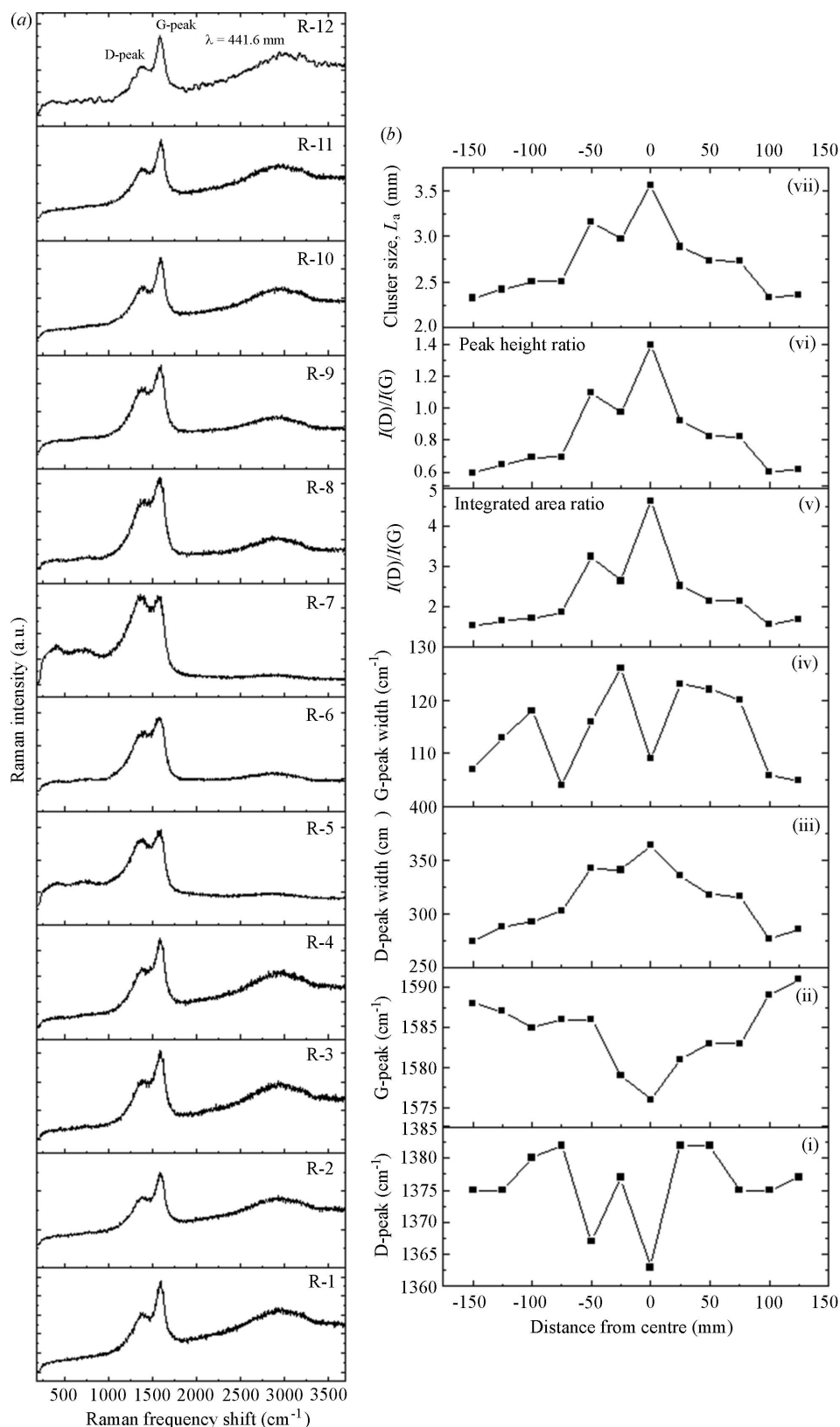


Figure 4 (a) Measured and fitted (Parratt formalism) reflectivity of the carbon-contaminated mirror at three different wavelengths (80, 90, 100 Å). Vertical dotted lines indicate the critical momentum transfer of carbon and gold. (b) The corresponding optical density profile.


Figure 6

(a) Raman spectra (R-1 to R-12) from the contaminated mirror surface in intervals of 25 mm along the long dimension of the mirror (see Fig. 3). Spectrum R-1 is from one edge of the mirror, spectrum R-7 from the centre (dense contaminated region) and R-12 from the other end of the mirror. (b) The corresponding cluster size (nm), $I(D)/I(G)$ ratios, D- and G-peak width and D- and G-peak positions calculated from Lorentzian fittings in the 900–2000 cm⁻¹ frequency range.

(1575–1590 cm⁻¹) and D (1362–1380 cm⁻¹) bands of carbon. These bands are generally present in all poly-aromatic hydrocarbons. This notation arises from the Raman spectra of nano-crystalline graphite, which generally shows two peaks. The D-mode at ~1360 cm⁻¹ is due to the A_{1g} symmetry mode at the K -point. The D-mode is caused by the disordered structure of graphene. The presence of disorder in sp^2 -hybridized carbon systems results in resonance Raman spectra, and thus makes Raman spectroscopy one of the most sensitive techniques for characterizing disorder in sp^2 carbon materials. This mode is forbidden in perfect graphite and only becomes active in the presence of disorder (Tuinstra & Koenig, 1970). The G-mode, at ~1580 cm⁻¹, is due to the E_{2g} symmetry mode at the Γ -point. The G-band arises from the stretching of the C–C bonds (sp^2) in graphitic materials, and is common to all sp^2 carbon systems whether they are arranged in rings or chains; this mode does not require the presence of six-fold rings. In amorphous C atoms a peak at around 1060 cm⁻¹ (T-peak) is seen in UV excitation. The cross section for amorphous sp^3 C–C vibrations is negligible for visible excitation, thus its Raman signature can only be seen for UV excitation (Ferrari & Robertson, 2001). For samples containing a significant fraction of diamond phase, the diamond sp^3 peak can be seen at 1332 cm⁻¹. The Raman scattering cross section of graphite (sp^2) and hydrogenated amorphous carbon (a-C:H) is approximately 50 and 230 times, respectively, higher compared with diamond carbon (sp^3) (Wada *et al.*, 1980; Sails *et al.*, 1996). So, visible Raman spectroscopy can only probe the configuration of sp^2 sites in sp^2 -bonded clusters. Nevertheless, it can be used to indirectly estimate the sp^3 -C fraction in cases where sp^2 clustering is affected by the sp^3 fraction, such as in a-C:H films. In the present case it is expected that the

layer has both sp^2 and sp^3 hybridized C atoms and the $sp^3:sp^2$ ratio can vary by the interaction of photons and secondary electrons. For a qualitative estimation the simplest approach is to fit the visible Raman spectra of a-C:H films, and from the intensity ratio $I(D)/I(G)$ it is possible to obtain a qualitative idea about the extent of sp^2 and sp^3 carbon bonding in the samples.

The D-mode is dispersive with photon excitation energy, even when the G-peak is not dispersive. The intensity of the D-peak is strictly connected to the presence of aromatic rings. For small grain/cluster size (L_a), the D-mode strength is proportional to the probability of finding a six-fold ring in the cluster that is proportional to the cluster size also. Thus, in amorphous C atoms the development of a D-peak indicates ordering, exactly the opposite of the case of graphite. For nano-crystalline materials the $I(D)/I(G)$ ratio is inversely proportional to the in-plane cluster size: L_a (nm) = $(560/E^4)[I(D)/I(G)]^{-1}$ (Tuinstra & Koenig, 1970; Knight & White, 1989); this relation is no longer valid for amorphous or hydrogenated amorphous C atoms (a-C/a-C:H). The modified relation $[I(D)/I(G) \propto L_a^2]$ for cluster size was proposed by Ferrari & Robertson (2000). The intensity of the D-band contains information about the ordered aromatic rings and not its width which again depends on the disorder. So, with the introduction of sp^2 -C sites in a-C:H, the D-peak height increases while its width increases/decreases depending on the ordering/disordering of the sp^2 sites. Thus, the peak area is less sensitive to a change in disorder compared with the peak height. So, it is more logical to use peak height ratios for $I(D)/I(G)$.

From data fittings of measured spectra (900–2000 cm^{-1}) we calculated the G and D positions and widths, the $I(D)/I(G)$ ratio from both peak heights as well as integrated peak areas and cluster size (shown in Fig. 6b). The graphs in Figs. 6(b-v) and 6(b-vi)] indicate that as we move from off centre to the central region (R-1 to R-7, low dose to high photon dose) the peak height ratio as well as the integrated peak areas ratio $I(D)/I(G)$ both gradually increase from 0.6 to 1.4 and 1.5 to 4.5, respectively. The $I(D)/I(G)$ ratio is an important parameter that measures disordering in crystalline and nano-crystalline C atoms and ordering in amorphous C atoms. The peak height ratios and integrated intensity ratios follow the same trend with different magnitude. Here we will use the peak height ratio for further calculations because the D-peak height is more sensitive to sp^2 sites compared with peak area. The $I(D)/I(G)$ ratio mainly increases by formation of sp^2 sites in the layer or we can say that sp^3 sites convert into sp^2 sites by interaction with photon/secondary electrons and arrange in the form of aromatic rings in the layer. We can understand this process as follows: initially when hydrocarbon molecules are adsorbed on the surface of the mirror they probably form long chains of hydrocarbon molecules, with the carbon atoms in both sp^3 and sp^2 hybridization states (ta-C:H and a-C:H) with fewer sp^2 sites in aromatic rings or chains. When photons fall and interact with these adsorbed hydrocarbon molecules containing C–H, C–C and C–O bonds, the bonds break and some dangling bonds are formed by abstraction of hydrogen

and oxygen. These highly reactive carbon atoms react with other highly reactive carbon atoms and form aromatic rings (sp^2 sites) and long chains. When we move from off centre to centre, the photon dose increases, the probability of bond breaking and formation of new dangling bonds increases, and as a result the probability of the formation of aromatic rings (sp^2 sites) increases, and thus the $I(D)/I(G)$ ratio increases. Faradzhev *et al.* also proposed a similar carbonaceous product reaction deduced from valence-band and GC/MS spectroscopic measurements made after EUV irradiation of adsorbed *n*-tetradecane on TiO_2 thin film (Faradzhev *et al.*, 2013). The increase in D-band width indicates that the aromatic rings are not perfectly ordered in the cluster, as the photon dose increased disorder in the clusters increases. For amorphous film the cluster size at different locations (R-1 to R-12) is calculated by use of the modified Tuinstra & Koenig relation (Tuinstra & Koenig, 1970; Ferrari & Robertson, 2000). The cluster size increases from 2.3 nm to 3.5 nm as we move from R-1 to R-7 and again decreases to 2.3 nm as we move from R-7 to R-12. From these observations we can conclude that, as the photon dose increases formation of sp^2 sites or aromatic rings, the cluster size and disordering in the deposited layer increase. Roy *et al.* also estimated the sp^2 -C to sp^3 -C fraction by $I(D)/I(G)$ measurements, and concluded that an increase in the sp^3 carbon fraction in a-C:H films not only decreases the number of sp^2 -C clusters but also their size in the nano-crystalline palladium interlayer (Si/nc-Pd/a-C:H) (Roy *et al.*, 2007; Tay *et al.*, 1998).

Figs. 6(b-v) and 6(b-vi) show changes in the G- and D-peak position from the off-centre region (R-1 and R-12) to the central region (R-7). When we move from off centre to centre (R-1 to R-7 or R-12 to R-7) the G- and D-peak positions change from 1590 cm^{-1} to 1576 cm^{-1} and 1375 cm^{-1} to 1363 cm^{-1} , respectively. The dispersion in the G- and D-peaks depends on the sp^2/sp^3 ratio, cluster size, content of H and phase of carbon, such as ta-C:H, a-C:H, nC-graphite *etc.*, in the layer. In the off-centre region where the photon flux is less, there may be the coexistence of hydrogenated amorphous carbon (a-C:H) and hydrogenated tetrahedral amorphous carbon (ta-C:H) with high number of C–H bonds. In the central region, due to the high photon flux, more hydrogen abstraction takes place and as a result the concentration of hydrogen decreases and the nature of the layer changes from ta-C:H to a-C:H with the formation of aromatic rings, thus the G- and D-peaks shift towards the lower side. Ferrari & Robertson (2000) also observed a shift in the G-peak position towards the lower side when the nature of the film changed from ta-C (85% sp^3 -C) to a-C (20% sp^3 -C). Dispersion in the G-peak (1587–1581 cm^{-1}) by increasing the number of graphene layers ($n = 1$ to 20) basically by an increase in cluster size (L_c) along the *c*-axis was also observed by Gupta *et al.* (2006). In the present sample near the central region (R-7) the carbon layer thickness is expected to be higher due to the conversion of C–H bonds into C–C bonds by high photon dose. The thickness of the carbon, about 400 Å, is measured by soft X-ray reflectivity. The out-of-plane cluster size ($L_c = 1.12$ nm) is calculated by peak fitting of the amorphous carbon

hump in the diffraction pattern measured at the angle-dispersive X-ray diffraction beamline of Indus-2.

C–H vibrational modes in amorphous carbon cannot be detected by visible Raman spectroscopy due to their high frequency. A second-order Raman effect from 2500 to 3300 cm^{-1} centered around 2920 cm^{-1} in all spectra is also observed. The source of this broad peak is the combined effect of 2D, 2G, G+D and CH_x stretching vibrations modes. Ferrari & Robertson (2000) detected CH_x stretching modes at 2920 cm^{-1} in polymeric a-C:H film by UV Raman spectroscopy. This broad peak gives an indication of the presence of C–H bonds or the presence of hydrogen in the layer. However, a typical signature of hydrogenated samples in visible Raman spectroscopy is the increasing photoluminescence background for increasing H content. This is due to the hydrogen saturation of non-radiative recombination centers. For H content over 40–50% this background usually overshadows the Raman signal of a-C:H (Marchon *et al.*, 1997; Casiraghi *et al.*, 2005). The presence of hydrogen in a-C:H thin films [deposited by different techniques such as plasma-enhanced chemical vapour deposition (PECVD), electron cyclotron wave resonance (ECWR) and distributed electron cyclotron resonance (DECR) with different process gases like CH_4 , C_2H_2] was estimated by Casiraghi *et al.* (2005) by the ratio of the slope of the fitted linear background to the intensity of the G-peak [$m/I(\text{G})$]. They reported that, when hydrogen content in the film increases from approximately 15% to 45%, the $m/I(\text{G})$ ratio increases from 0.6 μm to 15 μm . Here, we also measured $m/I(\text{G})$ ratios for all spectra from R-1 to R-12 (see Fig. 7). The $m/I(\text{G})$ ratio continuously decreases from 1.77 μm (R-1) to 0.19 μm (R-7) and again increases to 1.93 in the R-12 region. If we compare these results with those of Casiraghi *et al.* (2005) it is found that this contamination layer shows a variation in hydrogen content from 25% to 15%. The reason for this variation (decrease in H content) is the variation in the distribution of photon dose on the mirror surface. As already discussed for the central region, the photon dose is highest and decreases continuously at the edges

of the mirror. A higher number of photons can break the large number of C–H bonds, thus higher hydrogen abstraction takes place.

4. Summary

We studied the nature of carbon deposition on a mirror surface in a synchrotron radiation environment. The contamination layer is characterized by Raman spectroscopy, soft X-ray reflectivity and grazing-incidence X-ray diffraction techniques. By Raman spectroscopy it is concluded that carbon on the mirror surface has both sp^3 - and sp^2 -hybridized states and spreads on the mirror surface in the form of chains and aromatic rings with small size clusters. In off-centre regions (R-1 and R-12) the numbers of rings (sp^2 -C) are less, as we move from off-centre to the central region due to the increase in photon dose sp^3 sites converting into sp^2 sites and more aromatic rings are formed. An increase in the $I(\text{D})/I(\text{G})$ ratio indicates that the size of the cluster as well as the number of rings in the cluster increases. The increase in the D-peak width indicates disordering in the cluster. The ratio of the slope of the linear background to the intensity of the G-peak [$m/I(\text{G})$] indicates that the layer has a distribution of hydrogen content varying from 25% to 15%. From soft X-ray reflectivity it is concluded that in the central region the contamination layer thickness is about 400 Å and the roughness of the layer is 60 Å. The density of the layer is 72% of bulk graphitic carbon. GIXRD indicates that the nature of the layer is amorphous. In conclusion it is observed that the contamination layer is a-C:H. The $sp^2:sp^3$ ratio, formation of aromatic rings, disordering and cluster size increase with photon dose, whereas hydrogen content decreases with photon dose.

Acknowledgements

The authors are thankful to Dr A. K. Sinha and Mr Manvendra Singh for their support in performing GIXRD experiments on the ADXR beamline. Miss Manglika Sinha is acknowledged for her support in the soft X-ray reflectivity measurements.

References

- Attwood, D. (1999). *Soft X-rays and Extreme Ultraviolet Radiation: Principles and Applications*. New York: Cambridge University Press.
- Boller, K., Haelbich, R. P., Hogrefe, H., Jark, W. & Kunz, C. (1983). *Nucl. Instrum. Methods Phys. Res.* **208**, 273–279.
- Casiraghi, C., Piazza, F., Ferrari, A. C., Grambole, D. & Robertson, J. (2005). *Diamond Relat. Mater.* **14**, 1098–1102.
- Choi, J. & Hatta, T. (2015). *Appl. Surf. Sci.* **357**, 814–818.
- Conway, N. M. J., Ferrari, A. C., Flewitt, A. J., Robertson, J., Milne, W. I., Tagliaferro, A. & Beyer, W. (2000). *Diamond Relat. Mater.* **9**, 765–770.
- Ellis, S. G. (1951). *Proceedings of the on Electron Microscope Society of America Annual Conference*, Washington, USA.
- Faradzhev, N. S., McEntee, M., Yates, J. T. Jr, Hill, S. B. & Lucatorto, T. B. (2013). *J. Phys. Chem. C*, **117**, 23072–23081.
- Ferrari, A. C. & Robertson, J. (2000). *Phys. Rev. B*, **61**, 14095–14107.
- Ferrari, A. C. & Robertson, J. (2001). *Phys. Rev. B*, **64**, 075414.

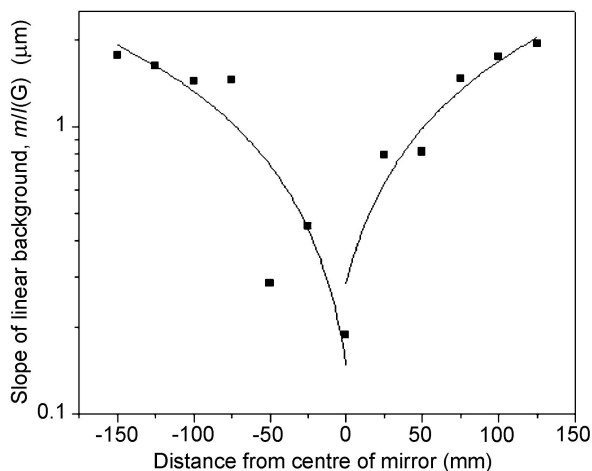


Figure 7
Ratio of the slope (m) of the linear background to the G-peak height $m/I(\text{G})$ (in μm) as a function of distance from the centre of the mirror.

- Ferrari, A. C. & Robertson, J. (2004). *Philos. Trans. R. Soc. A*, **362**, 2477–2512.
- Gupta, A., Chen, G., Joshi, P., Tadigadapa, S. & Eklund, P. C. (2006). *Nano Lett.* **6**, 2667–2673.
- Hart, R. K., Kassner, T. F. & Maurin, J. K. (1970). *Philos. Mag.* **21**, 453–467.
- Hollenshead, J. & Klebanoff, L. (2006). *J. Vac. Sci. Technol. B*, **24**, 64–82.
- Knight, D. S. & White, W. B. (1989). *J. Mater. Res.* **4**, 385–393.
- Leontowich, A. F. G. & Hitchcock, A. P. (2012). *J. Vac. Sci. Technol. B*, **30**, 030601.
- Marchon, B., Jing, Gui., Grannen, K., Rauch, G. C., Ager, J. W., Silva, S. R. P. & Robertson, J. (1997). *IEEE Trans. Magn.* **33**, 3148–3150.
- Nandedkar, R. V., Sawhney, K. J. S., Lodha, G. S., Verma, A., Raghuvanshi, V. K., Sinha, A. K., Modi, M. H. & Nayak, M. (2002). *Curr. Sci.* **82**, 298–304.
- Parratt, L. G. (1954). *Phys. Rev.* **95**, 359–369.
- Robertson, J. (2002). *Mater. Sci. Energ.* **37**, 129–281.
- Roy, M., Mali, K., Joshi, N., Misra, D. S. & Kulshreshtha, S. K. (2007). *Diamond Relat. Mater.* **16**, 517–525.
- Sails, S. R., Gardiner, D. J., Bowden, M., Savage, J. & Rodway, D. (1996). *Diamond Relat. Mater.* **5**, 589–591.
- Sinha, A. K., Sagdeo, A., Gupta, P., Upadhyay, A., Kumar, A., Singh, M. N., Gupta, R. K., Kane, S. R., Verma, A. & Deb, S. K. (2013). *J. Phys. Conf. Ser.* **425**, 072017.
- Tay, B. K., Shi, X., Tan, H. S., Yang, H. S. & Sun, Z. (1998). *Surf. Coat. Technol.* **105**, 155–158.
- Tuinstra, F. & Koenig, J. L. (1970). *J. Chem. Phys.* **53**, 1126–1130.
- Wada, N., Gaczi, P. J. & Solin, A. (1980). *J. Non-Cryst. Solids*, **543**, 35–36.
- Yadav, P. K., Modi, M. H., Swami, M. K. & Singh, P. J. (2016). *J. Electron Spectrosc. Relat. Phenom.* **211**, 64–69.